World Electric Vehicle Journal

MDPI

Article

Flicker-Free LED Driver Based on Cuk Converter with Integrated Magnetics

Yanxia Shen *, Jintao Xia and Chengchao Cai

Engineering Research Center of Internet of Things Technology Applications Ministry of Education, Jiangnan University, Wuxi 214122, China
* Correspondence: shenyx@jiangnan.edu.cn; Tel.: +86-138-6186-7517

Abstract: Electric vehicles contain various types of light emitting diode (LED) devices. A significant twice-line-frequency ripple current is usually produced in a conventional offline LED driver with a high power factor. In this paper, a flicker-free LED driver based on isolated Cuk converter with integrated magnetic technique is proposed. Two inductors and power transformer are combined into one magnetic core to eliminate the wave current as much as possible. With time domain analysis in electrical circuit and magnetic circuit, the operation principle, operational waveforms, and transfer function are analyzed in detail. Finally, experimental results from a 30 W laboratory prototype supplied by a 220 V grid validate the effectiveness of proposed LED driver.

Keywords: lighting emitting diode; cuk converter; flicker-free; magnetic integration

Citation: Shen, Y.; Xia, J.; Cai, C. Flicker-Free LED Driver Based on Cuk Converter with Integrated Magnetics. *World Electr. Veh. J.* **2023**, *14*, 75. https://doi.org/10.3390/wevj14030075

Academic Editors: Mario Marchesoni and Alfonso Damiano

Received: 16 January 2023
Revised: 20 February 2023
Accepted: 17 March 2023
Published: 19 March 2023

1. Introduction

Light emitting diodes (LEDs) have the advantages of long lifetime, high luminous efficiency, small size, energy saving, and environmental friendliness. It has gradually become the fourth generation of green light source following incandescent, fluorescent, and sodium lamps [1–3]. With the improvement of light efficiency and chromatic aberration, LED is widely used in electric vehicles, screen display, and other fields. LEDs require a constant DC current to produce stable lighting. Therefore, the LED driver is the most critical part of the entire LED lighting equipment, which determines the quality of the lighting and seriously affects the sales price of the entire lighting equipment, the use of expenditure and service life. High-quality LED driver is a guarantee for the development of the LED industry, which directly affects the performance of LED.

To satisfy the harmonic standard in IEC 61000-3-2 with AC power supply such as general lighting and large-screen display, a power factor correction (PFC) stage is required in LED driver. Generally, PFC stage can be Fly-back, Buck, Buck-Boost, SEPIC, et al. All of these single-stage LED drivers have only once power conversion, which has high efficiency, small size, and is controlled simply [4–6]. While the power conversion achieves unity power factor, the input current is in the same phase as the input voltage, and the instantaneous input power takes on twice-line-frequency, which results in pulsating current in LED [7]. For example, if the grid frequency is 50 Hz, the LED will contain current component with 100 Hz. Studies in recent years have found that long-term learning and working under the flickering light will lead to fatigue easily [8,9]. At the same time, the pulsating current generated by the LED driver can also affect the stability and efficiency of the overall system operation of electric vehicles powered by electricity.

The diodes in the circuit not only produce losses, but also reduce the power factor of the circuit. Because the rectifier bridge is composed of four uncontrollable ordinary diodes, each diode has a threshold voltage (generally 0.5 V for silicon, 0.2 V for germanium). The AC power passing through the diode rectifier bridge causes waveform distortion, which is no longer an ideal sine wave, and the voltage waveform is used as a reference for the back-end PFC control circuit to correct the input current, which makes the input current

also occur over the zero distortion, the input power factor of the circuit is reduced, and the higher harmonics at the zero point of the input voltage are increased. In addition, while the PFC circuit works, the input current will flow through three semiconductor devices (two rectifier diodes and a switching tube or two rectifier tubes plus the renewal diode) at any given time, the circuit components experience large through-state losses, which are more pronounced in the case of low-voltage and high current diode through-state losses.

To eliminate AC components in offline LED drivers, scholars have focused on two main aspects: one is optimizing topology structure, the other is improving control strategy. In [10], a bidirectional Buck-Boost converter is connected in parallel between the fly-back converter and LED load. The bidirectional Buck-Boost converter provides a path for the AC component pulsating current with twice line frequency of the PFC converter to flow through, leaving a pure DC current to drive the LED load without flicker. The principle of the bidirectional converter is to absorb the second harmonic AC ripple current of the PFC converter [11]. But two switches are needed in this topology and the two control loops will increase the complexity of the design. The number of system components, cost, and size can be significantly reduced using schemes such as PSR [12].

In [13], a LED driving circuit based on Cuk with active ripple compensation is proposed. In this circuit, the active ripple compensation branch is used to replace the output filter's electrolytic capacitor to offset the inductor ripple current, which provides the LED array with a constant DC and further with an ideal driving state. There are many strengths among the proposed LED driver, such as high reliability, suitable for a wide range of voltages, small volume by integrating compensation circuit and control circuit. But this method is only suitable for a low-power LED with a DC input voltage and requires a DC source for the transistor. In [14], electrolytic capacitors are also eliminated and a flyback three-port converter is used to make the driver smaller and the control strategy simpler.

In [15], a new control strategy is proposed to reduce the peak-to-average ratio of the instantaneous input power by injecting third and fifth harmonics in the input current. The variation of the duty cycle in a line period of fly-back converter is derived in a DCM mode and is further simplified for ease of implementation, requiring only the sensing of the input voltage. However, a drawback of the harmonic injection techniques is that two control loops are needed, which increases the complexity of the control structure compared with the conventional LED driver. On the other hand, if the capacitance value is reduced further, it is necessary to increase the amplitude of the harmonics, which will reduce the power factor [16]. Additional power processing circuitry at the converter output port is required to compensate for output current combined with voltage ripple to improve the power factor [17,18]. However, IEC 1000-3-2 requires that the maximum third harmonic amplitude should be less than 0.3 *I**PF if the input power is larger than 25 W. Therefore, this method is only suitable for small power supply. Moreover, a complicated control approach, more stress on the semiconductor devices, and a high switching frequency, result in higher losses and poor efficiency.

According to the principle of luminescence of LED, a flicker-free offline LED driver based on Cuk converter with integrated magnetics is proposed in this paper. Two inductors and isolated transformer are integrated into one magnetic core so that a certain proportion of the voltage can supply to the two inductors. This approach allows a zero current ripple in theory by means of a proper design of inductors and transformer, thus resulting in low cost, small volume, and high power density.

The remaining of this paper is organized as follows. Section 2 introduces the principle of the Cuk converter with integrated magnetics. Section 3 presents the procedure of the small signal modeling and transfer function of the converter. In Section 4, the design of the circuit is shown. Section 5 presents simulation and experimental results according to the designed parameter. Finally, the conclusion of this work is detailed in Section 6.

2. Operating Principle

Figure 1 shows the circuit configuration of the proposed flicker-free LED driver based on isolated Cuk converter with integrated magnetic technique. The isolated Cuk converter includes switch Q_1, inductors L_1 and L_2, the coupling capacitors C_1 and C_2 with large voltage ripple, diode D_1, transformer T_r in which L_P and L_S are the primary and secondary inductance of the transformer, and LED load. The transformer T_r is introduced to separate the input and output. The two inductors and the transformer are wound on an EI magnetic core to achieve magnetic integration. In the proposed circuit, the transformer wire is wound around the center leg3, and two conductors' wire are wound around the two side leg—leg1 and leg2 with a very small air gap. Mutual inductance exists between the two inductors by this method and ensures decoupling integration between the two inductors and the transformer. Due to the mutual inductance, the voltage can be shared and the voltage on the inductors can be reduced [19,20]. Then the twice-line-frequency LED current ripple of the LED driver based on the Cuk converter with integrated magnetics can be greatly reduced.

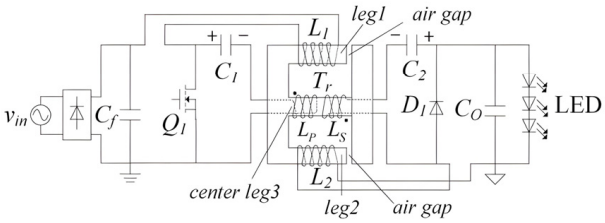

Figure 1. Topology of the flicker-free LED driver with integrated magnetics.

Compared with Buck-Boost converter and SEPIC converter, Cuk converter has the following advantages.

1. Both input and output are connected to inductors, making both input and output currents continuous and the pulsating currents of both are small, which is convenient for filtering at the input and output.
2. The output voltage of Cuk converter can be larger or smaller than the input voltage, which increases the application range of the converter.
3. The Cuk converter has better anti-interference performance because the switching tube short-circuits the interference at the input during the switching tube conduction and the diode short-circuits the interference at the input during the switching tube turn-off.
4. If the input inductor and output inductor are integrated into one core, the output ripple can be reduced by half, and by choosing a suitable inductor value or increasing the operating frequency of the converter, the output current can theoretically achieve zero ripple.

The circuit operates in continuous conduction mode (CCM) because the Cuk CCM inverter has a medium power capacity, ability to step up or down, and low input/output current ripples [21]. The flicker-free LED driver is operated in two modes based on its operation principle: (1) Q_1 switched on and D_1 switched off and (2) Q_1 turned off and D_1 turned on. Figure 2 shows the equivalent circuit of proposed LED driver in each mode of operation. Figure 3 shows the key voltage and current waveforms.

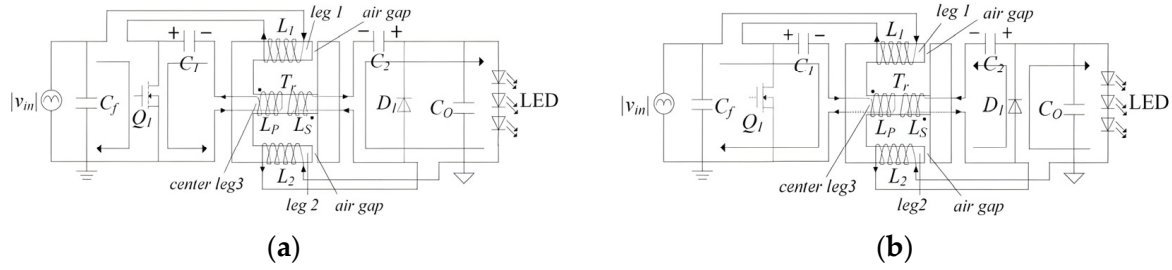

Figure 2. The equivalent circuit of the proposed LED driver. (**a**) [t_0–t_1]. (**b**) [t_1–t_2].

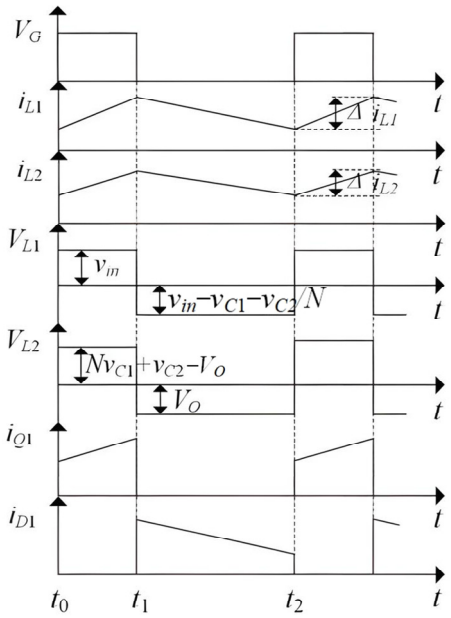

Figure 3. The key waveforms of voltage and current.

To simplify the analysis process, the following assumptions are made:

1. All electronic devices are ideal, ignoring their parasitic parameters.
2. The switching frequency f_S is much larger than the grid frequency f_L, that is to say the input voltage is approximately constant over a switching period;
3. Capacitors C_1, C_2, and C_O are large enough to keep the voltage constant approximately;
4. Since the decoupling integration mainly affects the volume and loss of the magnetic components, the influence on voltage and current is very small, the interaction between the inductors and the transformer can be neglected.

Mode1 [t_0–t_1]: At t_0, the switch Q_1 is turned on and diode D_1 is turned off because of the reverse voltage. The equivalent circuit is shown in Figure 2a. The voltage on the inductor L_1 is input voltage v_{in} and it is charging during this period. The voltage on the primary winding N_L is equal to the voltage of the capacitor C_1. At the same time, the voltage induced by the secondary winding N_S and capacitor C_2 supplies to LED load together. The current flowing through L_2 increases and L_2 stores energy. According to Figure 2a, the equation can be expressed as

$$\begin{cases} V_{L1} = L_1 \frac{di_{L1}}{dt} + M \frac{di_{L2}}{dt} = v_{in} \\ V_{L2} = L_2 \frac{di_{L2}}{dt} + M \frac{di_{L1}}{dt} = NV_{C1} + V_{C2} - V_O \end{cases} \quad (1)$$

where V_{L1} and V_{L2} are the voltages on the L_1 and L_2 respectively, V_{C1} and V_{C2} are the voltages on the C_1 and C_2 respectively, M is the mutual inductance between L_1 and L_2, $N = N_S/N_P$ is the transformer turns ratio.

Mode2 [t_1–t_2]: At t_1, the switch Q_1 was turned off and diode D_1 was turned on to provide an afterflow for L_S and L_2. At this time, L_1 is discharging and provides energy to C_1. Meanwhile, the voltage induced by the secondary winding is charging C_2 through D_1. L_2 provides energy to LED load through D_1 as well. According to Figure 2b, the equation can be expressed as

$$\begin{cases} V_{L1} = L_1 \frac{di_{L1}}{dt} + M \frac{di_{L2}}{dt} = v_{in} - V_{C1} - \frac{V_{C2}}{N} \\ V_{L2} = L_2 \frac{di_{L2}}{dt} + M \frac{di_{L1}}{dt} = -V_O \end{cases} \tag{2}$$

According to the volt-second balance for the inductors (L_1, L_2) over a switching period T_S, we can get

$$\begin{cases} Dv_{in} + (1-D)(v_{in} - V_{C1} - \frac{V_{C2}}{N}) = 0 \\ D(NV_{C1} + V_{C2} - V_O) + (1-D)(-V_O) = 0 \end{cases} \tag{3}$$

where D is the duty ratio of the switch Q_1.

The relationship between the input and output voltage can be expressed by the equation

$$\frac{V_O}{v_{in}} = \frac{ND}{1-D} \tag{4}$$

Substituting (1) and (3) into (4), the ripple currents can be derived as

$$\Delta i_{L2} = \frac{NL_1 - M}{L_2 - NM} \Delta i_{L1} \tag{5}$$

where Δi_{L1} and Δi_{L2} are the increment of i_{L1} and i_{L2} from t_0 to t_1.

From Equation (5), it is shown that if $M = NL_1$, the ripple current of the inductor L_2 reaches zero, and the input current i_{L1} remains the same as the case of no coupling. Therefore, the output current ripple is only related to inductor L_1, the mutual inductance M between two inductors, and the transformer turns ratio N. The mutual inductance M is an intrinsic parameter between the coils and related to the turns of the inductors, the dimension, the position, and the magnetic medium. Anyhow, the output current ripple can be much smaller than that of the discrete magnetics.

Therefore, according to the above working principle, the twice-line-frequency LED current ripple of the LED driver based on Cuk converter with integrated magnetics can be reduced greatly.

3. Critical Design Parameter

In this section, the critical design parameters of the proposed LED driver is discussed.

3.1. Inductors L_1 and L_2

As mentioned in Section 1, the LED driver is devised to operate in full CCM. Therefore, the design of the inductors L_1 and L_2 must ensure this operating condition so that all the relationships established in the theoretical analysis are valid. From (4), we have

$$D = \frac{V_O}{V_O + Nv_{in}} \tag{6}$$

In order to achieve high power factor, the maximum ratio of the current ripple through L_1 is chosen as 20%. According to the increase of i_{L1} from t_0 to t_1, the expression is shown in (7)

$$\frac{v_{in}}{L_1} DT_S < \frac{0.2P_O}{\eta v_{in}} \tag{7}$$

where η is the efficiency of LED driver, P_O is the power of LED, T_S is the switching period of Q_1 and $T_S = 1/f_S$.

Substitute (6) into (7) yields

$$L_1 > \frac{\eta V_O T_S v_{in}^2}{0.2 P_O (V_O + N v_{in})} \tag{8}$$

The average current flowing through the filter capacitor C_O is zero in a grid period, so the current flowing through the LED load is equal to the current flowing through L_2 and the maximum ratio of the current ripple through L_2 is chosen as 5%. The expression is shown in Equation (9)

$$\frac{V_O}{L_2}(1 - D)T_S < \frac{0.05 P_O}{V_O} \tag{9}$$

Substitute (6) into (9) yields

$$L_2 > \frac{N v_{in} T_S V_O^2}{0.05 P_O (V_O + N v_{in})} \tag{10}$$

3.2. Capacitors C_1, C_2, and C_O

The charging and discharging current of the filter capacitor C_O equal to the current ripple of L_2, which results in the voltage ripple on C_O. The equation of output voltage ripple is shown as (11).

$$\Delta V_O = \frac{1}{C_O} \Delta i_O t = \frac{1}{C_O} \Delta i_O (1 - D) T_S \tag{11}$$

The maximum voltage ripple on C_O is 0.1 V_{CO}

$$\Delta V_O < 0.1 V_O \tag{12}$$

Combining (11) and (12), the restriction of design C_O is obtained as

$$C_O > \frac{(1 - D)^2}{0.1 L_2 f_S^2} \tag{13}$$

Capacitors C_1 (is equal to C_2) transfers energy from input to output and in order to balance the instantaneous input and output power, the maximum voltage ripple on C_1 (or C_2) is 0.5 V_{C1} (or 0.5 V_{C2}). The computational procedure is same as C_O.

$$C_1 > \frac{(1 - D)^2}{0.5 L_1 f_S^2} \tag{14}$$

In practical design, C_1, C_2, and C_O are CBB capacitor because of low loss, low absorption coefficient, good frequency characteristic, good self- healing effect, and high reliability [22].

3.3. MOSFET Q_1 and Diode D_1

The maximum current flowing through Q1 is at the moment before Q1 is turned on and equals to the sum of IL1 and IC1. The calculation procedure of IQ is as follows.

$$I_Q = I_{L1} + I_{C1} = I_{L1} + N I_{C2} \tag{15}$$

$$I_{C2} = I_{L2} = \frac{1 - D}{ND} I_{L1} \tag{16}$$

$$I_Q = I_{L1} + \frac{1 - D}{ND} I_{L1} = \frac{1}{D} I_{L1} \tag{17}$$

The maximum voltage applied on the power switch transistor Q occurred at the moment after Q is turned on. The calculation procedure of VQ is as follows.

$$V_Q = v_{in} - V_{L1} \tag{18}$$

$$V_{L1} = -\frac{D}{1-D} v_{in} \tag{19}$$

$$V_Q = \frac{1}{1-D} v_{in} \tag{20}$$

The design procedures of the current flowing through D_1 and voltage applied on D_1 are similar to that of transistor Q. According to the above analysis, the circuit specifications and parameters designed in this paper are listed in Table 1.

Table 1. The key parameters of the proposed driver.

Parameter	Value
Input voltage v_{in_RMS}/V	220
Switching frequency f_S/Hz	100 k
Inductor L_1/mH	1.6 (30 Ts)
Inductor L_2/mH	2.4 (42 Ts)
Transformer turn ratio N_P:N_S	60:12
Capacitor C_1, C_2/μF	2.2 (650 V/CBB)
Filter capacitor C_O/μF	10 × 2 (160 V/CBB)
Output voltage V_O/V	33
Output current I_O/mA	900
Duty cycle D	0.31

4. Small-Signal Analysis and Controller Design

While the steady-state analyses define the DC status of the proposed circuit, the small-signal analysis is helpful in understanding the dynamic behavior of the integrated magnetic technique in the LED driver, and therefore, in determining the design criteria for a suitable controller and compensator. The state-space averaging method is a typical small-signal modeling and analysis method for power converters [23]. Compared with magnetic path-electric circuit paring transformation and gyrator-capacitor equivalent model [24], the magnetic-electrical circuit synthesis time domain model has one state variable less than the above two modeling methods, which greatly simplifies the derivation process of solving the transfer function with multi-order determinant [25]. Therefore, magnetic-electrical circuit synthesis time-domain model is suitable for establishing a small signal model of the isolated Cuk converter with integrated magnetic technique.

There are various methods for modeling switching converters, such as current injection equivalent circuit method, state space averaging method, switching element averaging model method, and switching network averaging model method. Among them, the state-space averaging method is to select the voltage or current parameters of the nonlinear components to derive a model independent of the switching frequency, which provides more intuitive input and output characteristics and is more physically meaningful. Therefore, the state-space averaging method is selected for the derivation and analysis of the small-signal model in this paper.

The reluctance model of the Cuk converter with integrated magnetic is shown in Figure 4. The L_1 is around the upper side leg1 with N_1 turns of conductor, the magnetic flux is φ_1, the reluctance is R_1; the L_2 is wound on the lower side leg2 with N_2 turns of conductor, the magnetic flux is φ_2, the reluctance is R_2; the primary and secondary side of the transformer are wound in center leg3 with the magnetic flux φ_C and the reluctance

R_C. Thus, according to Ohm's law based on the magnetic circuit, we can get the following equation:

$$\begin{cases} N_1 i_{L1} = N_2 i_{L2} + R_2\phi_2 + R_1\phi_1 \\ N_1 i_{L1} = R_C\phi_C + R_1\phi_1 \end{cases} \tag{21}$$

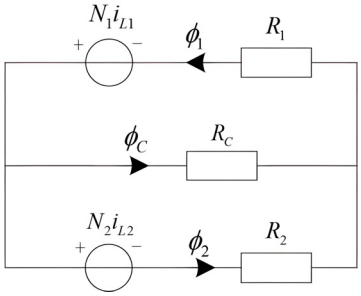

Figure 4. Reluctance model of the proposed circuit.

According to the continuity of magnetic flux, $\varphi_1 = \varphi_2 + \varphi_C$, then (6) can be rewritten as

$$\begin{cases} i_{L1} = \frac{(R_C+R_1)\phi_1 - R_C\phi_2}{N_1} \\ i_{L2} = \frac{R_C\phi_1 - (R_C+R_2)\phi_2}{N_2} \end{cases} \tag{22}$$

Select state vector $x(t)$ in the proposed Cuk converter as $[\phi_1(t)\ \phi_2(t)\ v_O(t)\ v_{C1}(t)\ v_{C2}(t)]^T$, the input variable $u(t)$ is $[v_{in}(t)]^T$, the state-space equation in mode 1 can be expressed as

$$\begin{cases} N_1 \frac{d\phi_1}{dt} = v_{in} \\ N_2 \frac{d\phi_2}{dt} = Nv_{C1} + v_{C2} - v_O \\ C_O \frac{dv_O}{dt} = i_{L2} - \frac{v_O}{R} \\ C_1 \frac{dv_{C1}}{dt} = Ni_{L2} \\ C_2 \frac{dv_{C2}}{dt} = i_{L2} \end{cases} \tag{23}$$

The findi Rewrite (8) as $\dot{x}(t) = Ax(t) + Bu(t)$, then A_1 and B_1 can be expressed as follows ngs and their implications should be discussed in the broadest context possible. Future research directions may also be highlighted.

$$A_1 = \begin{bmatrix} 0 & 0 & 0 & 0 & 0 \\ 0 & 0 & -\frac{1}{N_2} & \frac{N}{N_2} & \frac{1}{N_2} \\ \frac{R_C}{N_2 C_O} & -\frac{R_C+R_2}{N_2 C_O} & -\frac{1}{RC_O} & 0 & 0 \\ \frac{NR_C}{N_2 C_1} & -\frac{N(R_C+R_2)}{N_2 C_1} & 0 & 0 & 0 \\ \frac{R_C}{N_2 C_2} & -\frac{R_C+R_2}{N_2 C_2} & 0 & 0 & 0 \end{bmatrix}$$

$$B_1 = \begin{bmatrix} \frac{1}{N_1} \\ 0 \\ 0 \\ 0 \\ 0 \end{bmatrix}$$

Similarly, the state-space equation in mode 2 can be expressed as

$$\begin{cases} N_1 \frac{d\phi_1}{dt} = v_{in} - v_{C1} - \frac{v_{C2}}{N} \\ N_2 \frac{d\phi_2}{dt} = -v_O \\ C_O \frac{dv_O}{dt} = i_{L2} - \frac{v_O}{R} \\ C_1 \frac{dv_{C1}}{dt} = -i_{L1} \\ C_2 \frac{dv_{C2}}{dt} = -\frac{i_{L1}}{N} \end{cases} \tag{24}$$

The corresponding matrix A_2 and B_2 are

$$A_2 = \begin{bmatrix} 0 & 0 & 0 & -\frac{1}{N_1} & -\frac{1}{NN_1} \\ 0 & 0 & -\frac{1}{N_2} & 0 & 0 \\ \frac{R_C}{N_2 C_O} & -\frac{R_C+R_2}{N_2 C_O} & -\frac{1}{RC_O} & 0 & 0 \\ -\frac{R_C+R_1}{N_1 C_1} & \frac{R_C}{N_1 C_1} & 0 & 0 & 0 \\ -\frac{R_C+R_1}{NN_1 C_2} & \frac{R_C+R_2}{NN_2 C_2} & 0 & 0 & 0 \end{bmatrix}$$

$$B_2 = \begin{bmatrix} \frac{1}{N_1} \\ 0 \\ 0 \\ 0 \\ 0 \end{bmatrix}$$

Using the state-space averaging method, then we get the transfer function in the form of Laplasse transform and the small signal model is derived as follows:

$$\begin{bmatrix} s & 0 & 0 & \frac{D'}{N_1} & \frac{D'}{NN_1} \\ 0 & s & \frac{1}{N_2} & -\frac{ND}{N_2} & -\frac{D}{N_2} \\ \frac{-R_C}{N_2 C_O} & \frac{R_C+R_2}{N_2 C_O} & s + \frac{1}{RC_O} & 0 & 0 \\ A_{41} & A_{42} & 0 & s & 0 \\ A_{51} & A_{52} & 0 & 0 & s \end{bmatrix} \begin{bmatrix} \widehat{\phi_1}(s) \\ \widehat{\phi_2}(s) \\ \widehat{v_0}(s) \\ \widehat{v_{C1}}(s) \\ \widehat{v_{C2}}(s) \end{bmatrix} = \begin{bmatrix} \frac{1}{N} \\ 0 \\ 0 \\ 0 \\ 0 \end{bmatrix} v_{in}(s) + \begin{bmatrix} \frac{V_{C1}}{N_1} + \frac{V_{C2}}{NN_1} \\ \frac{NV_{C1}+V_{C2}}{N_2} \\ 0 \\ \frac{N\Delta_2}{N_2 C_1} \\ \frac{\Delta_2}{N_2} \end{bmatrix} \hat{d}(s) \tag{25}$$

where D' is the proportion of mode 2.

$$A_{41} = \frac{-ND}{N_2 C_1} R_C + \frac{D}{N_1 C_1}(R_1 + R_C)$$

$$A_{42} = \frac{ND}{N_2 C_1}(R_2 + R_C) - \frac{D'}{N_1 C_1} R_C$$

$$A_{51} = \frac{-D}{N_2 C_2} R_C + \frac{D'}{NN_1 C_2}(R_1 + R_2)$$

$$A_{52} = \frac{D}{N_2 C_2}(R_2 + R_C) - \frac{D'}{NN_1 C_2} R_C$$

Based on the above small-signal model, the duty- ratio-to-output-voltage transfer function G_{vd} (s) can be expressed as

$$G_{vd}(s) = \frac{\hat{v}(s)}{\hat{d}(s)} = \frac{a_1 s^3 + a_2 s^2 + a_3 s + a_4}{b_1 s^5 + b_2 s^4 + b_3 s^3 + b_4 s^2 + b_5 s + b_6} \tag{26}$$

where the derived parameters $a_i (I = 1, 2, 3, 4)$ and $b_j (j = 1, 2, 3, 4, 5, 6)$ are omitted for brevity.

In the model, the reluctance R_1 is 9.5 × 10^9 A·t/Wb, reluctance R_2 is 1.27 × 10^{10} A·t/Wb, reluctance R_C is 1.14 × 10^{10} A·t/Wb. Finally, we can calculate the $G_{vd}(s)$ based on MATLAB with the parameters in Table 1. The Bode diagram of $G_{vd}(s)$ is shown in Figure 5.

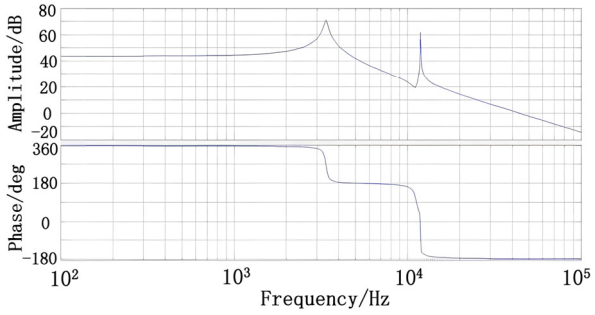

Figure 5. Bode diagram of $G_{vd}(s)$.

According to the Bode diagram, there are two low-frequency resonance points f_1 = 3.2 kHz and f_2 = 10.4 kHz and one zero resonance point f_3 = 10.6 kHz. The zero resonance point at f_3 balances the pole at f_2, so there is no resonance peak in the Bode diagram, the circuit phase lags by 180 degree and its amplitude-frequency characteristic is declining by 40 dB/dec. Therefore, to make the circuit stable when wide range input voltage, phase compensation circuit should adopt the type II feedback network.

Figure 6 shows the circuit diagram of a typical type II feedback network. In order to realize quick regulation and high PF, the voltage-mode control is adopted. The compensator transfer function is

$$G_{PI}(s) = \frac{K_{PI}(1 + \frac{s}{\omega_{Z1}})}{s(1 + \frac{s}{\omega_{P1}})} \tag{27}$$

where $K_{PI} = \frac{1}{R_1(C_3+C_f)}$, $\omega_{Z1} = \frac{1}{R_f C_f}$, $\omega_{P1} = \frac{C_3+C_f}{R_f C_f C_3}$.

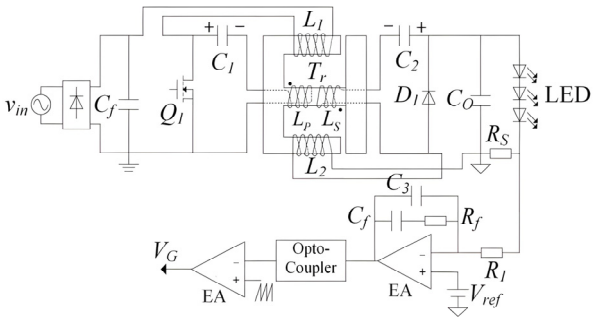

Figure 6. Proposed circuit with type II feedback network.

In this compensator design, the circuit parameters are R_1 = 51 kΩ, R_f = 270 kΩ, C_3 = 680 pF, C_f = 470 nF.

According to classical control theory, an ideal control system should have the following characteristics.

1. The low frequency band decreases at a slope of −20 dB/dec and has a certain height to ensure that the requirements of steady-state accuracy are met, followed by a slope of −40 dB/dec to increase the rapidity of the system.
2. The middle frequency band should ensure that the cut-off frequency is large enough to meet the requirements of dynamic rapidity, and the amplitude-frequency characteristic curve at the 0 dB line should cross at −20 dB/dec and maintain a certain width to meet the requirements of the relative stability of the system.

3. The amplitude-frequency characteristic curve of the high-frequency band should have a large negative slope, generally less than or equal to −40 dB/dec to improve the system's ability to resist high-frequency interference.

Figure 7 shows the Bode diagrams of the proposed compensator. It can be observed that ratio is −20 dB/dec in low frequency, −40 dB/dec in medium frequency, and −20 dB/dec in high frequency, which are the key characteristic according to classical control theory.

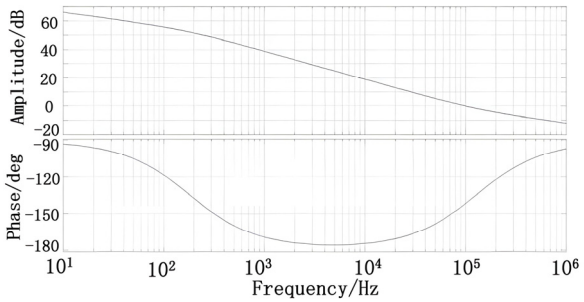

Figure 7. Bode diagrams of the proposed compensator.

5. Simulation and Results Analysis of Proposed LED Driver

The Saber software was used to simulate the Cuk circuit with integrated magnetics. A resistance was used instead of the LED. The parameters are listed in Table 1. All the diodes are ideal.

The simulation results of the magnetic integrated circuit are shown in Figure 8. Figure 8a shows the waveforms of input voltage v_{in} and input current i_{in}. It can be seen that the input voltage and current are nearly in the same phase, so the driver achieves unity power factor. Figure 8b shows the waveforms of the inductor current i_{L1}, i_{L2} and diode current i_{D1}. It can be seen that the circuit works in CCM mode. Figure 8c gives the flux curves of the three legs. Obviously, $\varphi_1 + \varphi_2 + \varphi_C = 0$, which is exactly the same as the theory.

In order to verify the proposed flicker-free LED driver, a prototype has been built and tested in the laboratory. Beside the parameters listed in Table 1, other specification of the prototype is as follows: the load is three strings of 10 × 1 W LED, the core of transformer adopts the EI-shaped ferrite magnetic, power switch Q_1:SPW20N60C3; free-wheeling diode D_1: HFA25TB60S; control IC: UCC3844.

The bridgeless Cuk converter studied in this paper is a small to medium power circuit, and the switching tubes used are MOSFETs, whose maximum current withstand value occurs at the moment of transition from mode 1 to mode 2. At the same time, the switch tube withstand voltage value needs to be considered to leave twice the margin. The above selection conditions were combined to select the Infineon SPW20N60C3 model with a drain breakdown voltage of 650 V, on-state resistance, and continuous drain current of 20.5 A (25 °C). The voltage stress of the diode is the same as the voltage of the switching tube, so the actual circuit should be left with more than twice the margin, the comprehensive selection of the international rectifier company HFA25TB60S. The UC3842 is a high-performance fixed-frequency current-mode PWM integrated controller from TI that uses a minimum of external components to achieve PFC correction and an internal high-current totem pole output of ±1 A, making it an ideal device for driving power MOSFETs.

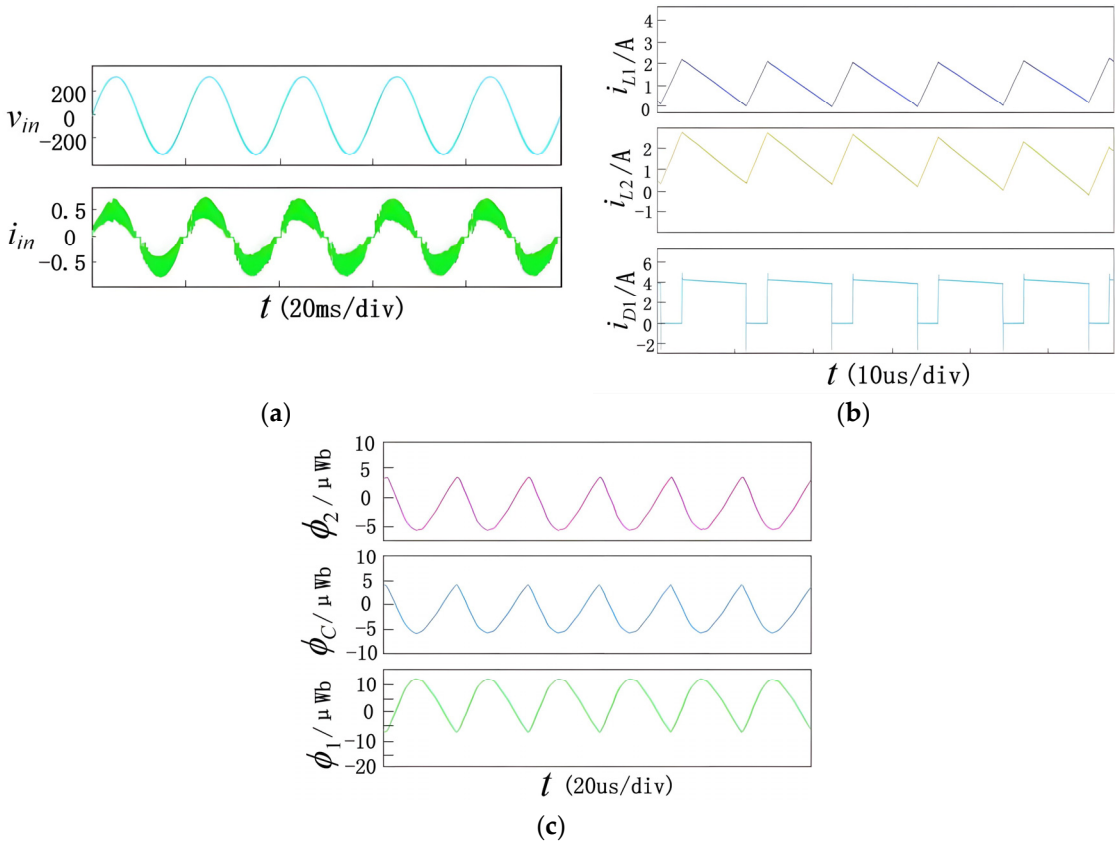

Figure 8. Simulation results of Cuk circuit with integrated magnetics. (**a**) Waveforms of v_{in} and i_{in}. (**b**) Waveforms of i_{L1}, i_{L2} and current i_{D1}. (**c**) Waveforms of φ_1, φ_2 and φ_3.

In addition, the filtering electrolytic capacitors required by the converter can be replaced by film capacitors or ceramic capacitors to some extent. Compared with electrolytic capacitors, film capacitors have the advantages of long life, high stability, good temperature characteristics, high voltage-withstanding capability, and low loss in high frequency, while ceramic capacitors have better high-frequency characteristics and can play the role of coupling, filtering, and oscillation in high-frequency circuits. Therefore, the use of film capacitors or ceramic capacitors can reduce the system loss and maintenance cost, while not affecting the size of the system.

Figure 9 shows the waveforms of input voltage v_{in} and current i_{in}. The input current follows the voltage change and achieves high power factor. The measured PF value is 0.982. Figure 10 shows the waveforms of switching signal VGS and the freewheeling diode current iD1. The switching frequency is presented as 100 kHz and the duty ratio D is 31%. The freewheel diode operates in CCM mode, which is exactly the same as the theoretical analysis. Figure 11 shows the waveforms of filter capacitor voltage V_O and LED current I_O. The filter capacitor voltage contains AC component with twice the line frequency, but the LED current is a pure DC current, thus it basically eliminates the LED flicker. Figure 12 shows a comparison of the system output current before and after the adoption of the magnetic integration technique. It can be seen that the system output current ripple is significantly reduced after adopting the integrated magnetic technology.

Figure 13 shows the relationship between the PF value and the efficiency of the flicker-free LED driver with different input voltage, respectively. From Figure 13, it can be seen that the PF value is always above 0.95 and the maximum efficiency is 0.838 over the entire input voltage range. The difference between the theoretical prediction and the experimental results occurs mainly due to the efficiency of the converter, which varies according to the input voltage. Figure 14 illustrates the winding method of the coil and transformer to form an integrated magnetic element, and the pin-out figure of the element. Figure 15 shows the

photo of the magnetic integrated inductance L1, L2 and transformer Tr. Figure 16 shows the system circuit diagram.

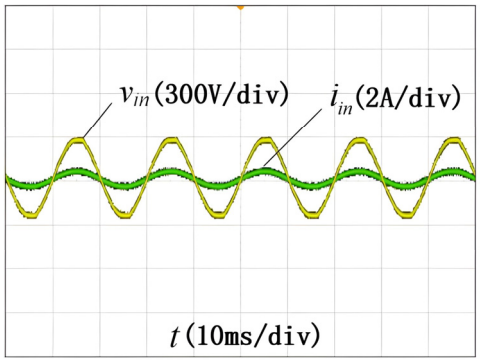

Figure 9. Waveforms of v_{in} and i_{in}.

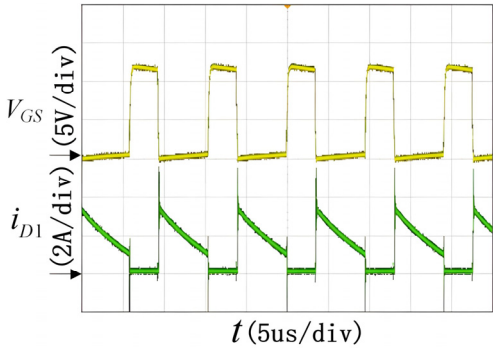

Figure 10. Waveforms of V_{GS} and i_{D1}.

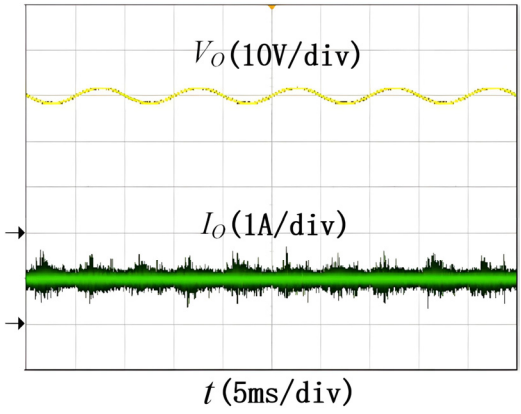

Figure 11. Waveforms of filter capacitor voltage V_O and LED current I_O.

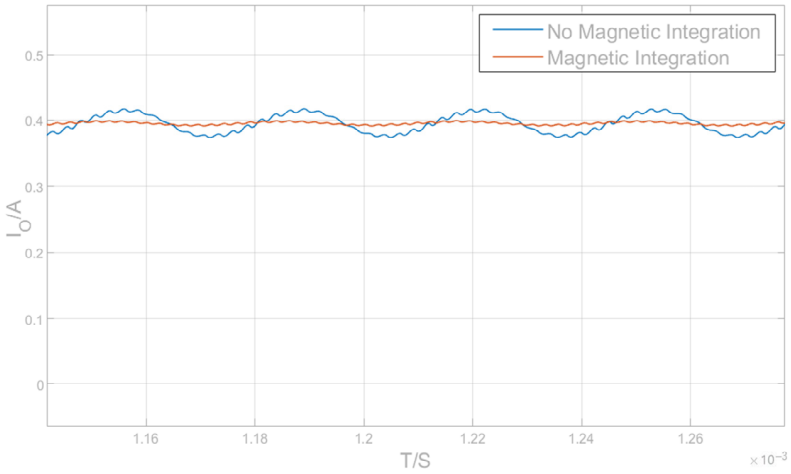

Figure 12. Comparison of output current before and after adopting integrated magnetic technology.

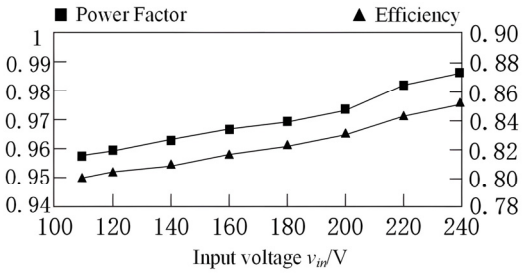

Figure 13. PF and efficiency of the proposed LED driver.

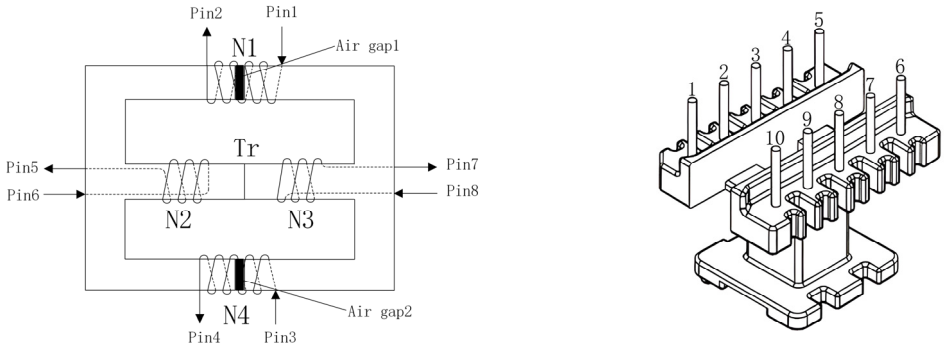

Figure 14. (**a**) The winding method of the coil. (**b**) The pin-out figure of the element.

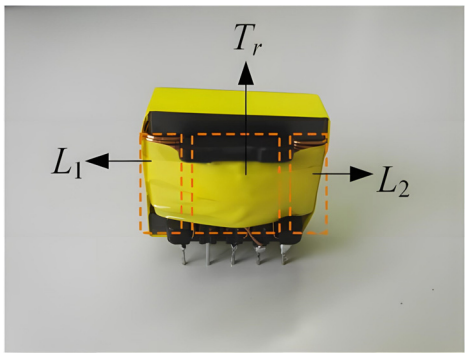

Figure 15. Photo of the magnetic integrated inductance and transformer.

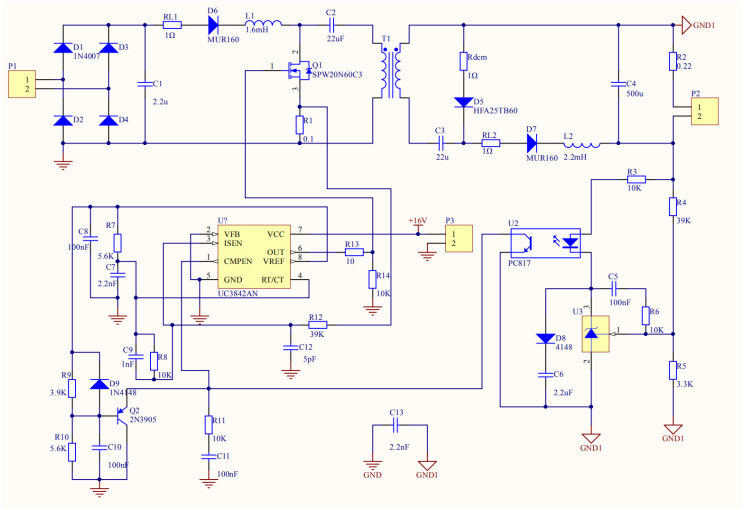

Figure 16. System circuit diagram.

The LED driver proposed in this paper reduces the cost of the system mainly through the following two aspects. First, in terms of component selection, film capacitors or ceramic capacitors can be used instead of the commonly used filtering electrolytic capacitors, which not only improves the system operating performance, but also saves component turnover and reduces system maintenance costs. Second, most current pulsating current elimination methods need to rely on complex control loops or require the provision of additional DC power supplies, etc. These methods more or less enhance the cost of building LED drivers. This paper proposes to integrate two inductors and isolation transformers in one core, which can make the maximum working magnetic density of the integrated magnetic parts much smaller than the magnetic density of each discrete magnetic parts and thus achieve the purpose of reducing the cross-sectional area of the magnetic parts core and reducing the cost and volume of the magnetic parts. At the same time, this approach does not need to rely on the above-mentioned measures to enhance system cost to achieve zero current ripple.

The converter efficiency can be improved by means of improving the magnetic concentration elements. There are two main types of methods to improve the magnetic concentration element with the main purpose of improving efficiency. The first type is to cut the AC fluxes to each other in the common column, which largely reduces the alternating magnetic density and at the same time reduces the loss of the magnetic core. There are three main ways: (1) Changing the winding connection and changing the coupling of fluxes; (2) merging the windings according to the specific circuit; (3) splitting the windings with the source transfer equivalent transformation method. The second type is the mutual superposition of AC flux and DC flux, which can improve the core utilization.

6. Conclusions

This paper presents a 30 W flicker-free LED driver prototype that uses magnetic integration technique to eliminate stroboscopic effect in an isolated Cuk converter. The operation principle of Cuk converter with integrated magnetics is analyzed in detail using time domain analysis in electrical and magnetic circuits. The transfer function Gvd (s) is calculated and the Bode diagram is drawn. Based on simulation and experimental results, the flicker-free LED driver has a power factor of 0.982 and a maximum efficiency of 0.838 when the input voltage is 240 V and LED current is pure DC current. The proposed driver is small-sized and cost-effective due to the use of only one transformer core. Future research will focus on improving the efficiency by analyzing the loss distribution of the magnetic integrated LED driver and applying a soft switching circuit and improved magnetic integrated element.

Author Contributions: Conceptualization, Y.S. and J.X.; methodology, J.X.; software, C.C.; validation, J.X.; formal analysis, all authors; investigation, all authors; writing—original draft preparation, Y.S.; writing—review and editing, J.X. and C.C.; visualization, C.C.; project administration, Y.S. and J.X.; funding acquisition, Y.S. and J.X. All authors have read and agreed to the published version of the manuscript.

Funding: This research was funded by the National Key R&D Program, grant number 2020YFB1711102.

Institutional Review Board Statement: Not applicable.

Informed Consent Statement: Not applicable.

Data Availability Statement: Not applicate.

Acknowledgments: The authors would like to thank all the anonymous reviewers for their insightful comments and constructive suggestions.

Conflicts of Interest: The authors declare no conflict of interest.

References

1. Liao, Z.; Ruan, X. Present status and developing trend of the semiconductor lighting. *Trans. China Electrotech. Soc.* **2006**, *21*, 106–111.
2. Marty, C.; Howard, C.; Ken, M. Solid-state lighting: Rhe new normal in lighting. *IEEE Trans. Ind. Appl.* **2015**, *51*, 109–119.
3. Sun, C.C.; Ma, S.H.; Nguyen, Q.K. Advanced LED Solid-state Lighting Optics. *Crystals* **2020**, *10*, 758. [CrossRef]
4. Behzad, P.; Ehsan, A. Analysis of the integrated SEPIC-Flyback converter as a single stage single-switch power-factor-correction LED driver. *IEEE Trans. Ind. Electron.* **2016**, *63*, 3562–3570.
5. Yan, T.; Xu, J.; Cao, T.; Zhou, G.; Gao, J. A flicker-free transformerless LED driving circuit based on quadratic Buck PFC converter. *Trans. China Electrotech. Soc.* **2015**, *30*, 512–519. [CrossRef]
6. Soares, G.M.; Almeida, P.S.; Alonso, J.M.; Braga, H.A.C. Capacitance minimization in offline LED drivers using an active ripple compensation technique. *IEEE Trans. Power Electron.* **2017**, *32*, 3022–3033. [CrossRef]
7. Peng, F.; Liu, Y.; Paresh, C. A flicker-free single-stage offline LED driver with high power factor. *IEEE J. Emerg. Sel. Top. Power Electron.* **2015**, *3*, 654–665. [CrossRef]
8. Wilkins, A.; Veitch, J.; Lehman, B. LED lighting flicker and potential health concerns: IEEE standard PAR1789 updatep. *IEEE Energy Convers. Congr. Expo.* **2010**, 171–178.
9. Lehman, B.; Wilkins, A.J. Designing to mitigate effects of flicker in LED lighting: Redcuing risks to health and safety. *IEEE Power Electron. Mag.* **2014**, *1*, 18–26. [CrossRef]
10. Wang, S.; Ruan, X.; Yao, K.; Tan, S.; Yang, Y.; Ye, Z. A flicker-free electrolytic capacitor-less AC-DC LED driver. *IEEE Trans. Power Electron.* **2012**, *27*, 4540–4548. [CrossRef]
11. Udumula, R.; Beeramangalla, L. Single-stage electrolytic capacitor less non-inverting buck-boost PFC based AC-DC ripple free LED driver. *IET Power Electron.* **2017**, *10*, 38–46.
12. Li, Y.; Chen, C. A novel primary-side regulation scheme for single-stage high-power-factor AC-DC LED driving circuit. *IEEE Trans. Ind. Electron.* **2013**, *60*, 4978–4986. [CrossRef]
13. Tang, Z.; Wang, R.; Yang, X. Power supply driven by Cuk constant current with active ripple compensation for LED headlamp. *J. S. China Univ. Technol.* **2016**, *44*, 34–39.
14. Wang, F.; Li, L.; Zhong, Y. An electrolytic capacitor-less LED driver with integrated dual flyback converter. *IEEE Trans. Ind. Electron.* **2017**, *64*, 5818–5827. [CrossRef]
15. Lamar, D.G.; Sebastian, J.; Arias, M. On the limit of the output capacitor reduction in power-factor correctors by distorting the line input current. *IEEE Trans. Power Electron.* **2012**, *27*, 1168–1176. [CrossRef]
16. Ma, H.; Zheng, C.; Yu, W.; Feng, Q. Electrolytic capacitor-less SEPIC-derived LED driver with valley fill cell. *Electr. Mach. Control.* **2012**, *16*, 13–20.
17. Sun, L.; Han, Y. A Capacitorless and Low-optical-flicker AC Direct LED Driving IC and System Applied to Street Lighting. *IEEE Trans. Electr. Electron. Eng.* **2021**, *16*, 1013–1024. [CrossRef]
18. Salazar-Perez, D.; Ponce-Silva, M.; Alonso, J.M.; Aqui-Tapia, J.A.; Cortes-Garcia, C. A Novel High-Power-Factor Electrolytic-Capacitor-Less LED Driver Based on Ripple Port. *IEEE J. Emerg. Sel. Top. Power Electron.* **2021**, *9*, 6248–6258. [CrossRef]
19. Chen, Q.; Feng, Y.; Zhou, L.; Wang, J.; Ruan, X. Active forward converter with integrated magnetics and the minimum output ripple current. *Proc. CSEE* **2009**, *29*, 7–13.
20. Khan, A.A.; Cha, H.; Kim, H.G. Magnetic Integration of discrete Coupled Inductors in Single-Phase Direct PWM AC-AC Converter. *IEEE Trans. Power Electron.* **2016**, *31*, 2129–2138. [CrossRef]
21. Han, B.; Lee, J.S.; Kim, M. Repetitive controller with phase-lead compensation for Cuk CCM inverter. *IEEE Trans. Ind. Electron.* **2016**, *65*, 2356–2367. [CrossRef]
22. Lam, J.; El-Taweel, N.; Abbasi, M. An output- current-dependent DC-link energy regulation scheme for a family of soft-switched AC/DC offline LED drivers without electrolytic capacitors. *IEEE Trans. Ind. Electron.* **2017**, *64*, 5838–5850. [CrossRef]

23. Nabinejad, A.; Rajaei, A.; Mardaneh, M. A Systematic Approach to Extract State-Space Averaged Equations and Small-Signal Model of Partial-Power Converters. *IEEE J. Emerg. Sel. Top. Power Electron.* **2020**, *8*, 2475–2483. [CrossRef]
24. Chen, Q.; Ruan, X.; Yang, Y. The application of the magnetic-integration techniques in switching power supply. *Trans. China Electrotech. Soc.* **2004**, *19*, 1–8.
25. Liu, Y.; Jiang, S.; Liang, W.; Wang, H.; Peng, J. Modeling and Design of the Magnetic Integration of Single- and Multi-stage EMI Filters. *IEEE Trans. Power Electron.* **2020**, *35*, 276–288. [CrossRef]